Case Studies in Thermal Engineering 12 (2018) 765–773

Contents lists available at ScienceDirect

Case Studies in Thermal Engineering

journal homepage: www.elsevier.com/locate/csite

Analysis of activation energy in magnetohydrodynamic flow with chemical reaction and second order momentum slip model

Aaqib Majeed[a,*], F.M. Noori[b], A. Zeeshan[c], T. Mahmood[d], S.U. Rehman[e], I. Khan[a]

[a] Department of Mathematics and Statistics, Bacha Khan University, Charsadda, KPK, Pakistan
[b] Department of Informatics, Faculty of Mathematics and Natural Sciences, University of Oslo, Oslo, Norway
[c] Department of Mathematics and Statistics, FBAS, IIUI, H-10, Islamabad 44000, Pakistan
[d] Department of Electronics Engineering, University of Engineering and Technology Taxila, Sub Campus Chakwal, Pakistan
[e] Department of Computer Science, University of Engineering and Technology Taxila, Sub Campus Chakwal, Pakistan

ARTICLE INFO

Keywords:
Activation energy
Binary chemical reaction
Second order slip
Heat transfer
Numerical study

ABSTRACT

This paper is communicated theoretically to study the collective effects of Arrhenius activation energy and binary chemically reactive species in the presence of the second order momentum slip model which has not been studied so far. To support these declaration in addition with electrically conducting boundary layer flow and heat transport have considered towards an exponential stretching sheet. The current study incorporates the impact of activation energy, temperature difference ratio parameter, 1st and 2nd order slip parameter, chemical reaction rate on fluid velocity, fluid temperature and concentration of chemical species are elaborated through graphically and discussed in detail. Appropriate transformations are betrothed to acquire nonlinear highly coupled ordinary differential equations (ODE's) from partial differential equations which are then solved numerically by employing finite difference collocation process that apply three-stage Lobatto IIIa scheme. The obtained results confirm that an excellent agreement is achieved with those available in open literature. It is found that concentration profile decreases in the presence of chemical reaction rate and temperature difference ratio parameter whereas opposite demeanour is seen for activation energy.

1. Introduction

The development of mass transfer phenomena with chemical reaction has attracted substantial interest to the researcher and scientists because of its innumerable useful applications in oil reservoir, chemical engineering, nuclear reactor cooling, geothermal engineering, deterioration of materials, mechano-chemistry, oil and water emulsions include Arrhenius activation energy along with the species binary chemical reactions. Usually the relation of chemical reactions with mass transfer are very complicated, and regularly it can be examined through fabrication and digestion of reactant species at dissimilar rates for both within the mass transfer and fluid flow. One of the most important benchmark is that typically not taken is the species chemical reactions along with Arrhenius activation energy. The terminology of activation energy was initially proposed by Arrhenius by [1]. He pronounced that least amount of energy (or threshold energy) is required to function atoms or molecules in a chemical system to flinch a chemical reaction. A simple model involving boundary layer fluid flow problem underneath binary chemical reaction with Arrhenius activation energy was first revealed by Bestman [2]. He applied perturbation technique to describe the activation energy impact in natural

* Corresponding author.
E-mail address: mjaaqib@gmail.com (A. Majeed).

https://doi.org/10.1016/j.csite.2018.10.007
Received 2 September 2018; Received in revised form 27 September 2018; Accepted 21 October 2018
Available online 26 October 2018

Nomenclature

A, B	Constant
C_p	Specific heat ($Jkg^{-1}K^{-1}$)
C_f	Skin friction
C_w	Wall concentration
C_∞	Ambient concentration
D	Mass diffusivity coefficient
E_a	Activation energy
E	Non-dimensional activation energy
f	Dimensionless stream function
M	Magnetic field (A/m)
m	Exponent fitted rate
k	thermal conductivity ($Wm^{-1}K^{-1}$)
K_n	Knudsen number
k_r^2	Exponential reaction rate
K_1	Boltzmann constant
L	Characteristic length
N_{ux}	Local Nusselt number
Pr	Prandtl number
R	Radiation parameter
Re_x	local Reynolds number
S	Suction/injection parameter
T	Temperature of the fluid (K)
T_w	Wall temperature
T_∞	Ambient free-stream temperature
U_w	Wall velocity
U_0	Reference velocity
Sc	Schmidt number
(u,v)	Velocity components (ms^{-1})
(x,y)	Coordinate axes normal to sheet (m)
μ	Dynamic viscosity (Nsm^{-1})
θ	Dimensionless temperature

Greek Symbols

γ	1st order slip
δ	2nd order slip
λ	Mean free molecular path
α	Momentum accommodation
ρ	Density (kgm^{-3})
σ	Chemical reaction rate constant
σ_1	Mean absorption coefficient
k^*	Absorption coefficient
Γ	Temperature difference parameter
ψ	Stream function (m^2s^{-1})

convection. Shafique et al. [3] scrutinised the mutual performance of activation energy and binary chemical reaction in rotating fluid flow over a stretching surface. Makinde et al. [4] examined the n^{th} order Arrhenius chemical reaction, thermal radiation, suction/injection, with buoyancy forces on unsteady incompressible fluid flow past a porous plate. Recently Zeeshan et al. [5] discussed the activation energy in Couette-Poiseuille flow in the presence of chemical reaction and convective boundary conditions. They employed HAM method to understand the problem.

The study of magneto-hydrodynamics (MHD) fluids are used in several industrial process to control the cooling rate. Moreover, nuclear reactor with cooling walls, fusing metals in electric heater, bearings and pumps, which are exaggerated with the collaboration between the conducting incompressible fluid and applied magnetics field. In eyesight of this, Pavlov [6] who primarily studied transvers magnetic field due to elastic deformation on plane surface using boundary layer approximation. Andersson [7] executed exact solution for the viscous fluid flow past a stretching surface under the impact of MHD. Ellahi et al. [8] examined 3D flow of Carreau fluid with magnetic field by applying homotopy analysis method. A generalized magnetic field impact on the flow of a Burgers' fluid model towards an inclined surface was elaborated by Rashidi et al. [9]. A numerical results of MHD viscous flow towards a permeable porous surface by applying successive linearization method (SLM) and Chebyshev spectral collocation method was adopted by Bhatti et al. [10]. Mukhopadhyay [11] investigated the thermally stratified medium surrounded with magneto hydrodynamic flow over an exponentially embedded. Mabood et al. [12] studied MHD viscous flow past an exponential stretching surface with radiation effects by applying Homotopy analysis method. Few investigations regarding the magnetic field over a stretchable surface can be stated through [13–20].

In all aforementioned literature survey, no-slip Navier boundary condition were considered, which is also recognized as a main principle of the Navier-Stokes philosophy [21]. Although, here some situation where slip condition is important. For example, Flow of gases below typical atmospheric pressure, in which slip conditions are useful in MEMS devices and low-pressure [22–24]. The 2-D steady mixed convection flow and heat transfer in ferromagnetic fluid under the influence of partial slip was explored by Zeeshan et al. [26]. Additionally, slip often arises in non-homogeneous fluid, particularly slurries, suspensions, gels, foams and emulsions [25]. Wu [26] has suggested a 2nd order slip model which is superior to the results of Fukui-Kaneko which are based on linearized Boltzmann equation [27]. Effects of MHD and slip on heat transfer boundary layer flow over a moving plate has been studied by Ellahi et al. [28]. Rashidi et al. [29] discussed the heat transport analysis over a stretchable surface under the impact of second order slip. Several authors adopted Wu's model to examine the influence of the liquid flow problems over a solid surfaces [30–32]. Some of the applications regarding to slip, MHD, against rarefied gases, sough surfaces and super hydrophobic micro-surfaces can be seen in more detail [33–39].

Inspired by the above investigation, the main persistence of our discussion is to explore the physical significance of activation energy with binary chemical reaction in the presence of 2nd order momentum slip model over an exponential stretching sheet because it has a tremendous application in micro systems like micro-valve, micro-nozzles, micro-pump and micro-electro-mechanical systems (MEMS) in flow regime. To the best of our information no such study has been described earlier.

2. Problem formulation

We have reflected 2-D incompressible electrically conducting viscous flow along an exponentially stretching sheet positioned at $y = 0$ along with both heat and mass transport characteristics. The x-axis and y-axis are taken along the coordinate axis and flow is occupied in the plane $y \geq 0$. Assume that the wall velocity of the plate is $U_w(x)$ in x-axis. Also assume that fluid temperature at wall is T_w which is greater than ambient temperature T_∞. A moveable magnetic field $B(x)$ is employed perpendicular to the horizontal. The induced magnetic field is flouted because of lower value of magnetic Reynolds number.

Under the above assumption with Boussinesq approximation, the governing equations of continuity, momentum energy and concentration are [40].

$$\frac{\partial u}{\partial x} + \frac{\partial v}{\partial y} = 0, \tag{1}$$

$$u\frac{\partial u}{\partial x} + v\frac{\partial u}{\partial y} = \upsilon\frac{\partial^2 u}{\partial y^2} - \frac{\sigma B^2}{\rho}u, \tag{2}$$

$$u\frac{\partial T}{\partial x} + v\frac{\partial T}{\partial y} = \alpha\frac{\partial^2 T}{\partial y^2} - \frac{1}{\rho c_p}\frac{\partial q_r}{\partial y}, \tag{3}$$

$$u\frac{\partial C}{\partial x} + v\frac{\partial C}{\partial y} = D\frac{\partial^2 C}{\partial y^2} - k_r^2\left(\frac{T}{T_\infty}\right)^m e^{\frac{-Ea}{K_1 T}}(C - C_\infty). \tag{4}$$

Here u, and v specifies the velocity component parallel to coordinate axis, ρ is the density of fluid, υ= notify the kinematic viscosity,α is the thermal diffusivity, C_p is the specific heat, $B(x) = B_o e^{x/2L}$ represent the variable magnetic field, B_o and T signify constant magnetic field and fluid temperature, C represent fluid concentration, D specify mass diffusivity coefficient, $k_r^2 = k_0^2 e^{x/2L}$ is the exponential reaction rate, $\left(\frac{T}{T_\infty}\right)^m e^{\frac{-Ea}{kT}}$ denote the Arrhenius function where m shows exponent fitted rate constants usually lies between $-1 < m < 1$.

The associated boundary equations corresponding to exponential stretching surface are

$$\left.\begin{array}{l} u = U_w(x) + U_{slip},\ v = -V(x),\quad T = T_w,\ C = C_w \ \text{ at} y = 0 \\ u \to 0,\ T \to T_\infty,\ C \to C_w \text{as} y \to \infty \end{array}\right\}. \tag{5}$$

Here $U_w(x) = U_o e^{x/L}$ expresses surface velocity, U_o is reference velocity, L is characteristic length, and $V(x) = V_o e^{x/L}$ is the special kind of velocity, where $V(x) < 0$ signify injection and $V(x) > 0$ represent suction. V_o is initial strength of suction, $T_w = T_\infty + T_o e^{x/2L}$ is fluid temperature at wall, T_o is reference temperature, $C_w = C_\infty + C_o e^{x/2L}$ indicate concentration at the sheet, C_o symbolise reference concentration at sheet, U_{slip} represent second order momentum slip model which is specified by Wu's [26]

$$\begin{aligned} U_{slip} &= \frac{2}{3}\left(\frac{3 - \alpha l^3}{\alpha} - \frac{2}{3}\frac{1 - l^2}{K_n}\right)\lambda\frac{\partial u}{\partial y} - \frac{1}{4}\left[l^4 + \frac{2}{K_n^2}(1 - l^2)\right]\lambda^2\frac{\partial^2 u}{\partial y^2} \\ &= A\frac{\partial u}{\partial y} + B\frac{\partial^2 u}{\partial y^2}. \end{aligned} \tag{6}$$

Here K_n is Knudsen number is stated as the ratio of molecular mean free path λ to a physical length for the flow, $l = \min(1/K_n, 1)$ and α is momentum adaptation coefficient with $0 \leq \alpha \leq 1$. From signification of l, we conclude that for every value of K_n, we take $0 \leq l \leq 1$. The molecular mean free path is always positive which give a negative result of B.

Now applying Rosseland approximation, radiative flux q_r is recognized as

Table 1
Calculated value of Nusselt number when $\delta = \gamma = Sc = E = S = \Gamma = \sigma = m = 0$.

M	R	Pr	Present results	Mabood et al. [12]	Ishak [32]
0	0	1	0.954783	0.95478	0.9548
		2	1.471460	1.47151	
		3	1.869073	1.86909	1.8691
		4	2.204512	2.50012	2.5001
		5	2.500131	–	–
		10	3.660371	3.66039	3.6604
0	1	1	0.531730	0.53121	
1	0		0.861109	0.86113	
0	0.5	2	1.073519	1.07352	1.0735
		3	1.380752	1.38075	1.3807
		4	1.640265	–	–
		5	1.869073	–	–
1	1	1	0.450571	0.450571	0.450571

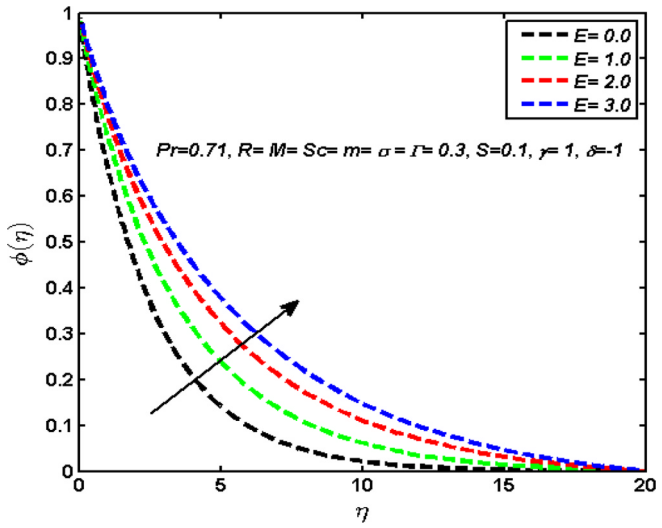

Fig. 1. Visualize the impact of activation energy (E) on $\phi(\eta)$.

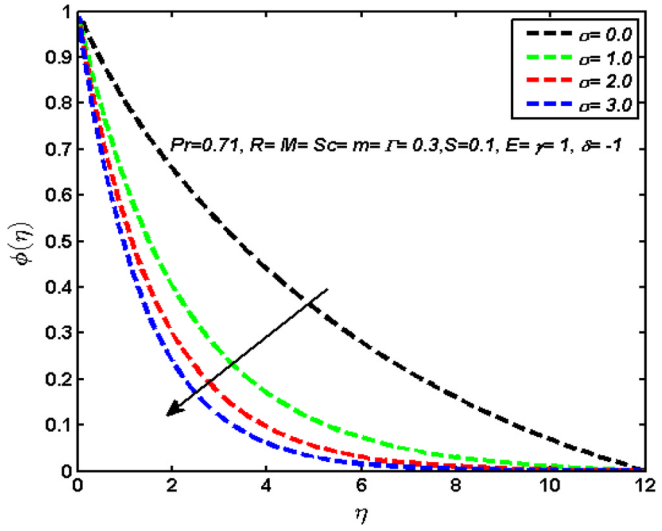

Fig. 2. Visualize the impact of chemical reaction rate (σ) on $\phi(\eta)$.

$$q_r = -\frac{4\sigma_1}{3k^*}\frac{\partial T^4}{\partial y}, \tag{7}$$

The temperature differences inside flow region are small enough, therefor T^4 can be obtained by expanding Taylor series around T_∞ and ignoring the terms of greater order

$$T^4 \approx 4T_\infty^3 T - 3T_\infty^4. \tag{8}$$

Substituting Eqs. (7) and (8) into (3), we find

$$u\frac{\partial T}{\partial x} + v\frac{\partial T}{\partial y} = \alpha\frac{\partial^2 T}{\partial y^2} + \frac{16\sigma T_\infty^3}{3\rho c_p k^*}\frac{\partial T}{\partial y^2}. \tag{9}$$

3. Method of solution

We introduce the transformation of the form

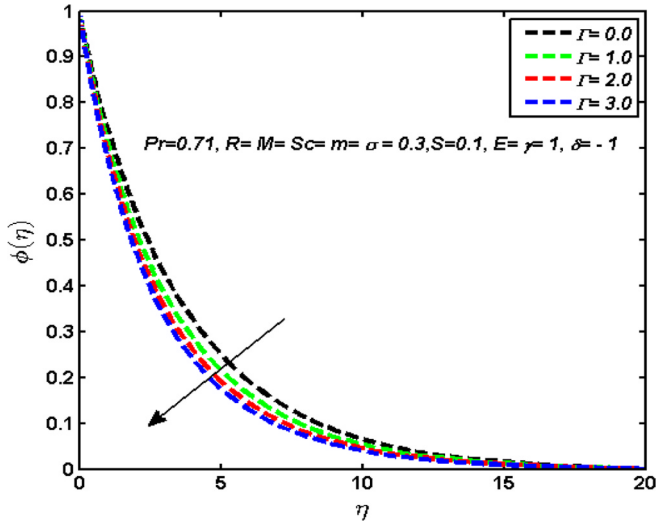

Fig. 3. Visualize the impact of Temperature difference ratio (Γ) on $\phi(\eta)$.

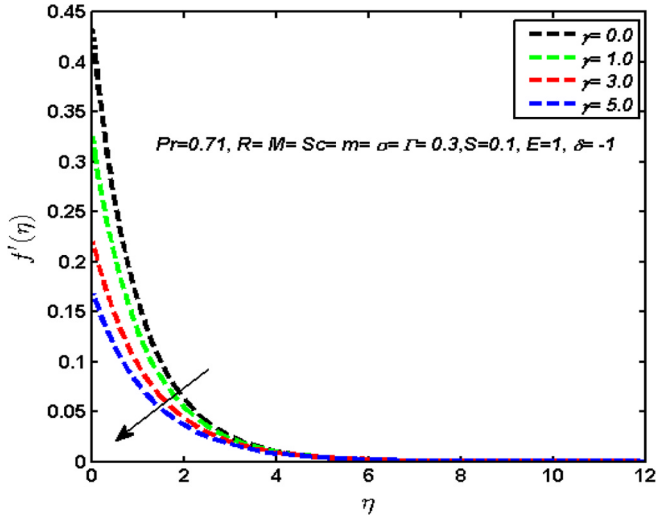

Fig. 4. Visualize the impact of first order slip parameter (γ) on $f'(\eta)$.

$$\eta = y\sqrt{\frac{U_o}{2\nu L}}e^{x/2L},\ \psi(x,y) = \sqrt{2U_0\nu L}\,e^{x/2L}f(\eta),\ u = U_o e^{x/L}f'(\eta),$$
$$v = -\sqrt{\frac{U_o\nu}{2L}}e^{x/2L}[f(\eta) + \eta f'(\eta)],\ \theta(\eta) = \frac{T - T_\infty}{T_w - T_\infty},\ \phi(\eta) = \frac{C - C_\infty}{C_w - C_\infty} \tag{10}$$

by substitution of (10) in Eqs. (2)–(4), yield the following ODE's

$$f''' + ff'' - 2f'^2 - Mf' = 0, \tag{11}$$

$$\left(1 + \frac{4}{3}R\right)\theta'' + \Pr\left(f\theta' - f'\theta\right) = 0, \tag{12}$$

$$\phi'' + Sc(f\phi' - f'\phi) - Sc\sigma(1 + \Gamma\theta)^m e^{\frac{-E}{(1+\Gamma\theta)}}, \tag{13}$$

with boundary equations are:

$$\begin{cases} f'(0) = 1 + \gamma f''(0) + \delta f'''(0), f(0) = S, \phi(0) = 1 \\ \theta(0) = 1, f'(\infty) = 0, \quad \theta(\infty) = 0, \ \phi(\infty) = 0. \end{cases} \tag{14}$$

Here 1st and 2nd order slip parameters are itemized as

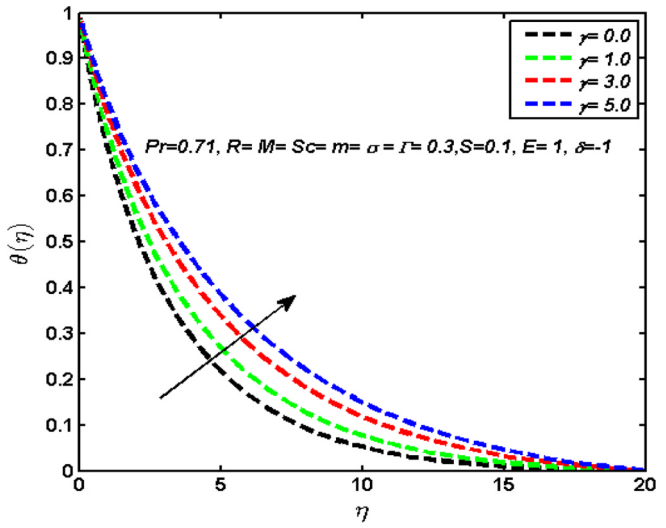

Fig. 5. Visualize the impact of first order slip parameter (γ) on $\theta(\eta)$.

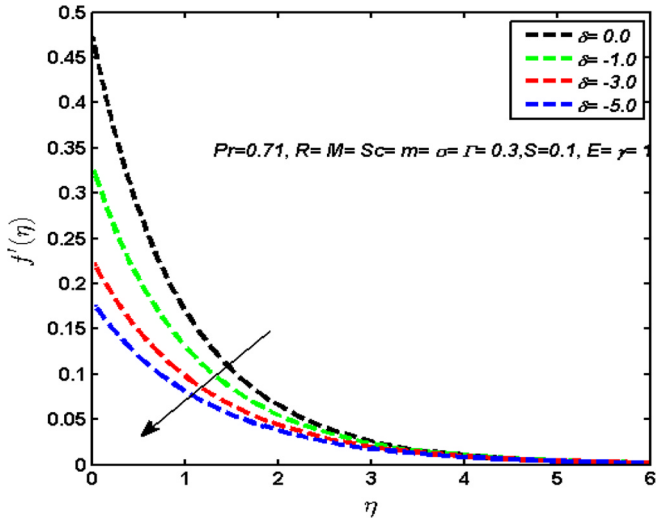

Fig. 6. Visualize the impact of second order slip parameter (δ) on $f'(\eta)$.

$$\left.\begin{aligned}\gamma &= A\sqrt{\frac{U_0}{2\nu L}}e^{x/2L} = \frac{2}{3}\left(\frac{3-\alpha l^3}{\alpha} - \frac{2}{3}\frac{1-l^2}{K_n}\right)\lambda\sqrt{\frac{U_0}{2\nu L}}e^{x/2L} > 0\\ \delta &= B\left(\frac{U_0 e^{x/L}}{2\nu L}\right) = -\frac{1}{4}\left[l^4 + \frac{2}{K_n^2}(1-l^2)\right]\lambda^2\left(\frac{U_0 e^{x/L}}{2\nu L}\right) < 0\end{aligned}\right\}. \tag{15}$$

Now Eqs. (11)–(13) together with Eq. (14) have a similarity solution. The parameters γ and δ are constant value and not depend on x as shown in Eq. (15). For this we set λ which is proportional to $e^{-x/2L}$, therefore we have

$$\lambda = ce^{-x/2L}, \tag{16}$$

here 'c' indicate constant of proportionality. By inserting of Eq. (16) into (15), we get

$$\left.\begin{aligned}\gamma &= \frac{2}{3}\left(\frac{3-\alpha l^3}{\alpha} - \frac{2}{3}\frac{1-l^2}{K_n}\right)\sqrt{\frac{U_0}{2\nu L}}c > 0\\ \delta &= -\frac{1}{4}\left[l^4 + \frac{2}{K_n^2}(1-l^2)\right]\left(\frac{U_0}{2\nu L}\right)c^2 < 0\end{aligned}\right\}. \tag{17}$$

The expression γ and δ stated Eq. (15), the solution of Eqs. (11)–(13) produce similar solutions. Whereas with γ and δ signify by relations (16), and consequently generated solutions are local similar solutions. Also $S = -V_o\sqrt{\frac{2L}{\nu U_0}} > 0(\text{or} < 0)$ denote the suction or injection parameter, $M = \frac{2\sigma B_0^2 L}{\rho U_o}$ represent magnetic parameter, $Pr = \frac{\nu}{\alpha}$ stands for Prandtl number, $R = \frac{4\sigma T_\infty^3 L}{kk^*}$ indicate radiation

parameter, $Sc = \frac{\nu}{D}$ is the Schmidt number, $\sigma = \frac{2lk_0^2}{u_0}$ is constant chemical reaction rate, $E = \frac{E_a}{K_1 T_\infty}$ is activation energy, $\Gamma = \frac{T_w - T_\infty}{T_\infty}$ is temperature relative parameter.

4. Physical quantities

The most significant relations of practical concern in the current analysis are friction factor, Sherwood number and heat transfer rate are

$$C_f = \frac{\mu \frac{\partial u}{\partial y}\Big|_{y=0}}{\rho (U_w)^2}, \; Nu = \frac{-x \frac{\partial T}{\partial y}\Big|_{y=0}}{k(T_w - T_\infty)}, \; Sh = \frac{-x \frac{\partial C}{\partial y}\Big|_{y=0}}{k(C_w - C_\infty)}. \tag{18}$$

Using the Eqs. (10) and (18) we have

$$\sqrt{\frac{2L}{x}}\, \mathrm{Re}_x^{1/2} C_f = f''(0), \; \sqrt{\frac{2L}{x}}\, Nu/\mathrm{Re}_x^{1/2} = -\theta'(0), \; \sqrt{\frac{2L}{x}}\, Sh/\mathrm{Re}_x^{1/2} = -\phi'(0), \tag{19}$$

here $\mathrm{Re}_x = \frac{U_w x}{\nu}$ designates local Reynolds number.

5. Numerical computation

The set of non-linear system of ODE's (11) to (13) along with appropriate boundary functions (14) were determined numerically by utilizing the Matlab software build in function bvp4c for various values of flow parameters. This software performs higher order finite difference method that usages collocation method which involves three-stage Lobatto IIIa scheme with forth-order accuracy. In this technique the ODE's are changed into a set of first order differential equations by considering similarity variables, the error and mesh size adjustment are depend on residual of the continuation solution.

The explanation of a collocation scheme (see Shampine et al. [41]) for two-point boundary value problem are:

$$x' = \psi(t, x), A \le t \le B, \tag{20}$$

along with boundary conditions

$$bc(x(A), x(B)) = 0. \tag{21}$$

The approximate solution S(t) is a continuous function that is a cubic polynomial on each subinterval $[t_n, t_{n+1}]$ of the mesh $A = t_0 < t_1 < t_2 ... < t_N = B$. It satisfies the boundary conditions

$$bc(S(A), S(B)) = 0, \tag{22}$$

and it also satisfies the following differential equations (collocates) at both ends and midpoint of each subinterval:

$$S'(t_n) = \psi(t_n, S(t_n)) = 0, \tag{23}$$

$$S'((t_n + t_{n+1})/2) = \psi((t_n + t_{n+1})/2, S(t_n + t_{n+1})/2) = 0, \tag{24}$$

$$S'(t_{n+1}) = \psi(t_{n+1}, S(t_{n+1})). \tag{25}$$

These conditions result in a system of nonlinear algebraic equations for the coefficients defining $S(t)$, which are solved iteratively by linearization. Here, $S(t)$ is a fourth-order approximation to an isolated solution $x(t)$, i.e., $\|x(t) - S(t)\| \le K\chi^4$, where χ is the maximum of step sizes $\chi_n = t_{n+1} - t_n$, and K is a constant. For such an approximation, the residual $r(x)$ in the ordinary differential equation is defined by

$$r(t) = S'(t) - \psi(t, S(t)) \tag{26}$$

In this approach, mesh selection and error control are based on the residual of the continuous solution. To obtain a good estimation, the relative error tolerance was set to 10^{-7}. The 'infinity' is interchanged by a fixed value $\eta = \eta_\infty = 30$. In fact present results illustrate a marvellous agreement between the data and gives us assurance for present code. For this we rewrite the above Eqs. (11)–(13) as

$$f''' = -ff'' + 2f'^2 + Mf', \tag{27}$$

$$\theta'' = -\frac{3\mathrm{Pr}}{(3 + 4R)}\left(f\theta' - f'\theta\right), \tag{28}$$

$$\phi'' = -Sc(f\phi' - f'\phi) + Sc\sigma(1 + \Gamma\theta)^m e^{\frac{-E}{(1+\Gamma\theta)}}, \tag{29}$$

we introduce the new variables in order to transform the above higher order differential equations into system of first order

$$y_1 = f, y_2 = f', y_3 = f'', y'_3 = f''',$$
$$y_4 = \theta, y_5 = \theta', y'_5 = \theta'', y_6 = \phi, y_7 = \phi', y'_7 = \phi'', \tag{30}$$

by inserting Eq. (30) into Eqs. (11)–(14), we get

$$\left.\begin{aligned} y'_1 &= y_2 \\ y'_2 &= y_3 \\ y'_3 &= -y_1 y_3 + 2y_2^2 + \mathrm{M} y_2 \\ y'_4 &= y_5 \\ y'_5 &= \tfrac{-3\mathrm{Pr}}{(3+4\mathrm{R})}(y_1 y_5 - y_2 y_4) \\ y'_6 &= y_7 \\ y'_7 &= -Sc(y_1 y_7 - y_2 y_6) + Sc\sigma(1+\Gamma y_4)^m e^{\frac{-E}{(1+\Gamma y_4)y_6}} \end{aligned}\right\}, \tag{31}$$

and

$$\left.\begin{aligned} &y_1(0) = S, y_2(0) = 1 + \gamma y_3(0) + \delta y'_3(0), \\ &y_4(0) = 1, y_6(0) = 1, y_2(\infty) = 0, y_4(\infty), y_6(\infty) = 0 \end{aligned}\right\}. \tag{32}$$

To solve (31) and (32) as an initial value problem, we prerequisite a values for $y_2(0)$, $y_3(0)$, $y_5(0)$, $y_7(0)$ that is, $f'(0)$,$f''(0)$, $\theta'(0)$ and $\phi'(0)$ these values are not given at the end point, which is automatically calculated with the present numerical technique in order to validate the far field boundary equations.

6. Results and discussion

The numerical simulations of the above transformed equations along with boundary equation are solved for numerous values of convergence flow parameters. In command to justify the validity of the present scheme, the present numerical results of Nussult number are compare with Mabood [12] and Ishak [32], which are displayed in Table 1. The results reveals a good agreement and shows accuracy of our method.

Fig. 1 visualize the impact of activation energy (??) on concentration profile. It is remarkably noticed that species concentration profile and their corresponding solute boundary layer thickness increases due to higher value of E. From practical point of view higher energy activation and weaker temperature leads to weaker rate of reaction, which slow down the chemical reaction.

Fig. 2 illustrates the behaviour of concentration profile for dissimilar results of chemical reaction rate (σ). From graph it is witnessed that species profile flattening inside the solute boundary layer. Because of increase in the rate of chemical reaction results in a thickening of mass transport boundary layer. When σ is gradually increasing. The factor $\sigma(1+\Gamma\theta)^m e^{\frac{-E}{(1+\Gamma\theta)}}$ is enhances due to increment in the values σ or m. Now the destructive reaction is encouraging owing to which species concentration increases. The influence of temperature ratio parameter (Γ) on concentration profile is portrayed in Fig. 3. Graph shows poor concentration profiles by increasing Γ and therefor reduces the concentration boundary layer thickness.

Figs. 4–5 designates the impact of 1st order slip parameter $0 \leq \gamma \leq 5$ on velocity and temperature profiles. Graphs elaborate that fluid velocity reduces in the boundary area with the increase of γ. This is due to fact that, once slip happens, the slippery of fluid indicates decrement in the surface among the viscous fluid and stretchable surface, in fact pulling forces cannot be partially transported to the fluid. On the other hand temperature profile within the flow field for dissimilar values of 1st order slip is exemplified in Fig. 5. Corresponding result shows that temperature profile enhances against first order slip. Fig. 6 represents the stimulus of 2nd order slip parameter (δ) on velocity profile. It is fascinating to observe that fluid velocity gradually slow down with the rise of absolute value of 2nd order momentum slip, it is also charming to comprehend that boundary layer becomes denser for lowest absolute value of 2nd order slip parameter.

7. Concluding remarks

Combined influence of Activation energy with binary chemical reaction with 2nd order velocity slip are considered for incompressible flow over an exponential stretching surface. The outcomes has been evaluated through graphs and tables. The main findings of the current analysis are:

- Concentration profile is an increasing function of E while it decreases for σ and Γ.
- Temperature profile enhances for higher first order slip parameter.
- Fluid velocity is flattening steadily with the increment of positive value of 2nd order slip whereas inverse trend is perceived for temperature profile.

Declaration

The author(s) declared no potential conflicts of interest with respect to the research.

References

[1] S. Arrhenius, Über die Dissociationswärme und den Einfluss der Temperatur auf den Dissociationsgrad der Elektrolyte, Z. Phys. Chem. 4 (1889) 96–116.
[2] A.R. Bestman, Natural convection boundary layer with suction and mass transfer in a porous medium, Int. J. Energy Res. 14 (1990) 389–396.
[3] Z. Shafique, M. Mustafa, A. Mushtaq, Boundary layer flow of Maxwell fluid in rotating frame with binary chemical reaction and activation energy, Results Phys. 6 (2016) 627–633.
[4] O.D. Makinde, P.O. Olanrewaju, W.M. Charles, Unsteady convection with chemical reaction and radiative heat transfer past a flat porous plate moving through a binary mixture, Afr. Mat. 22 (2011) 65–78.
[5] A. Zeeshan, N. Shehzad, R. Ellahi, Analysis of activation energy in Couette-Poiseuille flow of nanofluid in the presence of chemical reaction and convective boundary conditions, Results Phys. 8 (2018) 502–512.
[6] K.B. Pavlov, Magnetohydrodynamic flow of an incompressible viscous fluid caused by deformation of a plane surface, Magn. Gidrodin. 4 (1974) 146–147.
[7] V.P. Andersson, MHD flow of a viscoelastic fluid past a stretching surface, Acta Mech. 95 (1992) 227–230.
[8] R. Ellahi, M.M. Bhatti, C.M. Khalique, Three-dimensional flow analysis of Carreau fluid model induced by peristaltic wave in the presence of magnetic field, J. Mol. Liq. 241 (2017) 1059–1068.
[9] M.M. Rashidi, Z. Yang, M. Awais, M. Nawaz, T. Hayat, Generalized magnetic field effects in Burgers' nanofluid model, PLos One 12 (1) (2017) e0168923.
[10] M.M. Bhatti, T. Abbas, M.M. Rashidi, A new numerical simulation of MHD stagnation-point flow over a permeable stretching/shrinking sheet in porous media with heat transfer, Iran J. Sci. Tech. Trans. A Sci. 41 (3) (2017) 779–785.
[11] S. Mukhopadhyay, MHD boundary layer flow and heat transfer over an exponentially stretching sheet embedded in a thermally stratified medium, Alex. Eng. J. 52 (2013) 259–265.
[12] F. Mabood, W.A. Khan, A.M. Ismail, MHD flow over exponential radiating stretching sheet using homotopy analysis method, J. King Saud. Univ. Eng. Sci. 29 (2007) 68–74.
[13] M.M. Rashidi, S. Abelman, N. Freidooni Mehr, Entropy generation in steady MHD flow due to a rotating porous disk in a nanofluid, Int. J. Heat. Mass Transf. 62 (2013) 515–525.
[14] M. Sheikholeslami, K. Vajravelu, M.M. Rashidi, Forced convection heat transfer in a semi annulus under the influence of a variable magnetic field, Int. J. Heat. Mass Transf. 92 (2016) 339–348.
[15] M.M. Rashidi, N. Kavyani, S. Abelman, Investigation of entropy generation in MHD and slip flow over a rotating porous disk with variable properties, Int. J. Heat Mass Transf. 70 (2014) 892–917.
[16] M.M. Rashidi, M. Ali, N. Freidoonimehr, F. Nazari, Parametric analysis and optimization of entropy generation in unsteady MHD flow over a stretching rotating disk using artificial neural network and particle swarm optimization algorithm, Energy 55 (2013) 497–510.
[17] M. Sheikholeslami, M.M. Rashidi, D.D. Ganji, Effect of non-uniform magnetic field on forced convection heat transfer of Fe3O4–water nanofluid, Com. Meth. Appl. Mech. Eng. 294 (2015) 299–312.
[18] A. Zeeshan, A. Majeed, C. Fetecau, S. Muhammad, Effects on heat transfer of multiphase magnetic fluid due to circular magnetic field over a stretching surface with heat source/sink and thermal radiation, Results Phys. 7 (2017) 3353–3360.
[19] A. Majeed, A. Zeeshan, R. Ellahi, Chemical reaction and heat transfer on boundary layer Maxwell Ferro-fluid flow under magnetic dipole with Soret and suction effects, Eng. Sci. Tech. Int. J. 20 (3) (2017) 1122–1128.
[20] M. Sheikholeslami, A. Zeeshan, A. Majeed, Control volume based finite element simulation of magnetic nanofluid flow and heat transport in non-Darcy medium, J. Mol. Liq. 268 (2018) 354–364.
[21] J. Zhu, L. Zheng, X. Zhang, Hydrodynamic plane and axisymmetric slip stagnation-point flow with thermal radiation and temperature jump, J. Mech. Sci. Tech. 25 (2011) 1837–1844.
[22] M. Gal-el-Hak, The fluid mechanics of micro-devices-the Freeman scholar lecture, Trans ASME J. Fluids Eng. (1999) 5–33.
[23] V.P. Shidlovskiy, Introduction to the Dynamics of Rarefied Gases, American Elsevier Publishing Company Inc, New York, 1967.
[24] G.C. Pande, C.L. Goudas, Hydromagnetic Rayleigh problem for a porous wall in slip regime, Astrophys. Space Sci. 243 (1996) 285–289.
[25] A. Zeeshan, A. Majeed, R. Ellahi, M.Z. Zia, Mixed convection flow and heat transfer in ferromagnetic fluid over a stretching sheet with partial slip effects, Ther. Sci. 22 (2018) 1–12.
[26] L. Wu, A slip model for rarefied gas flows at arbitrary Knudsen number, Appl. Phys. Lett. 93 (2008) (Article ID 253103).
[27] S. Fukui, R. Kaneto, A database for interpolation of Poiseuille fl ow rates for high Knudsen number lubrication problems, J. Tribol. 112 (2008) 78–83.
[28] R. Ellahi, S.Z. Alamri, A. Basit, A. Majeed, Effects of MHD and slip on heat transfer boundary layer flow over a moving plate based on specific entropy generation, J. Taibah Univ. Sci. (2018) 1–7.
[29] M.M. Rashidi, A.A. Hakeem, N.V. Ganesh, B. Ganga, M. Sheikholeslami, E. Momoniat, E, Analytical and numerical studies on heat transfer of a nanofluid over a stretching/shrinking sheet with second-order slip flow model, Int. J. Mec. Mat. Eng. 11 (1) (2016).
[30] G. Singh, A.J. Chamka, Dual solutions for second-order slip flow and heat transfer on a vertical permeable shrinking sheet, Ain Shams Eng. J. 4 (2013) 911–917.
[31] A.V. Rosca, I. Pop, Flow and heat transfer over a vertical permeable stretching/shrinking sheet with a second-order slip, Int. J. Heat. Mass Transf. 60 (2013) 355–364.
[32] A. Ishak, MHD boundary layer flow due to an exponentially stretching sheet with radiation effect, Sains Malays. 40 (2011) 391–395.
[33] F. Sharipov, V. Seleznev, Data on internal rarefied gas flows, J. Phys. Chem. (1998) 657–706.
[34] C.H. Choi, C.J. Kim, Large slip of aqueous liquid flow over a nanoengineered superhydrophobic surface, Phys. Rev. Lett. 96 (2006).
[35] C.O. Ng, C.Y. Wang, Stokes shear flow over a grating: implications for superhydrophobic slip, Phys. Fluids 21 (2009).
[36] M.M. Bhatti, M.M. Rashidi, Effects of thermo-diffusion and thermal radiation on Williamson nanofluid over a porous shrinking/stretching sheet, J. Mol. Liq. 221 (2016) 567–573.
[37] C.Y. Wang, Stagnation slip flow and heat transfer on a moving plate, Chem. Eng. Sci. 61 (2006) 7668–7672.
[38] A. Majeed, A. Zeeshan, R.S.R. Gorla, Convective heat transfer in a dusty ferromagnetic fluid over a stretching surface with prescribed surface temperature/heat flux including heat source/sink, J. Natl. Sci. Found. Sri Lanka 46 (2018) 399–409.
[39] R. Ellahi, The effects of MHD and temperature dependent viscosity on the flow of non-Newtonian nanofluid in a pipe: analytical solutions, Appl. Mat. Mod. 37 (2013) 1451–1467.
[40] A. Bejan, Convection Heat Transfer, 2nd ed., Wiley, New York, 1995.
[41] L.F. Shampine, I. Gladwell, S. Thompson, Solving ODEs with Matlab, Cambridge University Press, 2003.